Published in final edited form as:
IEEE Trans Biomed Eng. 2012 October ; 59(10): 2705–2715. doi:10.1109/TBME.2012.2204749.

Behavior of Tip-Steerable Needles in *ex vivo* and *in vivo* Tissue

Ann Majewicz,
Department of Mechanical Engineering, Stanford University, Stanford, CA 94305 USA

Steven P. Marra,
Department of Mechanical Engineering, Johns Hopkins University, Baltimore, MD 21218 USA

Mark G. van Vledder,
Now with the Department of Surgery, Erasmus Medical Center, Rotterdam, 3015 CE, The Netherlands

MingDe Lin,
Clinical Site Researcher with Interventional Guidance Technology, Philips Research North America, Briarcliff, NY 10510 USA

Michael A. Choti,
Department of Surgery, Surgical Oncology Division, Johns Hopkins Medical Institutions, Baltimore, MD 21287 USA

Danny Y. Song, and
Departments of Radiation Oncology, Urology, and Oncology, Johns Hopkins Medical Institutions, Baltimore, MD 21287 USA

Allison M. Okamura
Department of Mechanical Engineering, Stanford University, Stanford, CA 94305 USA

Ann Majewicz: amajewi1@stanford.edu; Steven P. Marra: marra@jhu.edu; Mark G. van Vledder: M.vanvledder@erasmusmc.nl; MingDe Lin: Ming.Lin@philips.com; Michael A. Choti: mchoti@jhmi.edu; Danny Y. Song: dsong2@jhmi.edu; Allison M. Okamura: aokamura@stanford.edu

Abstract

Robotic needle steering is a promising technique to improve the effectiveness of needle-based clinical procedures, such as biopsies and ablation, by computer-controlled, curved insertions of needles within solid organs. In this paper, we explore the capabilities, challenges, and clinical relevance of asymmetric-tip needle steering though experiments in *ex vivo* and *in vivo* tissue. We evaluate the repeatability of needle insertion in inhomogeneous biological tissue and compare *ex vivo* and *in vivo* needle curvature and insertion forces. Steerable needles curved more in kidney than in liver and prostate, likely due to differences in tissue properties. Pre-bent needles produced higher insertion forces in liver and more curvature *in vivo* than *ex vivo*. When compared to straight stainless steel needles, steerable needles did not cause a measurable increase in tissue damage and did not exert more force during insertion. The minimum radius of curvature achieved by pre-bent needles was 5.23 cm in *ex vivo* tissue, and 10.4 cm in *in vivo* tissue. The curvatures achieved by bevel tip needles were negligible for *in vivo* tissue. The minimum radius of curvature for bevel tip needles in *ex vivo* tissue was 16.4 cm; however, about half of the bevel tip needles had negligible curvatures. We also demonstrate a potential clinical application of needle steering by targeting and ablating overlapping regions of cadaveric canine liver.

I. Introduction

A. Background and Motivation

Needle-based procedures are commonly used for medical diagnosis and intervention when there exists a nearly straight-line path between an entry point and subsurface target.

Examples of needle-based procedures include biopsy, ablation, and brachytherapy. For many procedures, accurate needle placement is critical for acquiring diagnostic samples and providing accurate delivery of therapy. However, tissue deformation can cause a straight needle to deviate from a desired path. Robotic needle steering is a promising technique that allows for correction of a needle path inside tissue, and may also enable new procedures currently not feasible with straight needles.

In the last decade, a number of needle steering techniques have been developed, along with associated mechanical models of needle-tissue interaction, path-planning algorithms, control strategies, and experiments to characterize parameters that affect needle steering in artificial and *ex vivo* tissue [1] [2] [3] [4] [5] [6] [7] [8] [9]. Complete needle steering systems, with integrated robotic devices, planners, and image-guided control, are also being developed and validated [10] [11] [4]. However, to become a clinically relevant technology, the usability of steerable needles to perform treatments in biological tissue must be demonstrated. No previous studies have measured steerable needle behavior in *in vivo* tissue, and our understanding of the repeatability of steerable needle insertion is far from complete.

In this paper we explore the capabilities, challenges, and clinical relevance of tip asymmetric needle steering in prostate, kidney, and liver. We present the first known work demonstrating needle steering in *in vivo* tissue (inside an intact, living organism) and conduct extensive needle insertion experiments *ex vivo* tissue (whole organs removed from an organism) to allow for statistical analysis of the effects of various parameters on tip-steerable needle behavior. Needle behavior includes needle curvature from three-dimensional needle reconstructions (CT or stereo X-ray) and insertion forces. We compare steerable needles to straight stainless steel needles and present a potential clinical application for needle steering for the treatment of large tumors with overlapping ablations.

This work uses a particular needle steering technique in which thin, flexible needle shafts curve during insertion due to tip forces induced by needle tip asymmetry. Our needle tips have either a simple bevel or a bevel combined with a permanent bend of the needle shaft very close to the tip. Control of the six-dimensional pose of the needle tip can be achieved by various patterns of needle insertion and rotation (spin about the needle's long axis), where rotation reorients the direction of asymmetry. In these experiments, we focus on the degree and repeatability of needle curvature, as well as needle insertion force.

B. Related Work

Previous needle steering experiments in *ex vivo* tissue include: studying needle-tissue interaction forces for bevel-tip needles in chicken breast [8], steering custom needles with large stainless-steel tips in cadaveric brain tissue [12], developing and testing an integrated active cannula and ablation device in *ex vivo* bovine liver [11]. Our preliminary work characterized the effects of various parameters on needle curvature in *ex vivo* goat liver [9]. *In vivo* forces associated with needle insertion have been measured for human prostate [13] [14], porcine liver [15], and both porcine liver and kidney [16]. However, the needles used in these experiments were conventional stainless steel needles. To date, the authors are not aware of any prior work to characterize steerable needle insertion in living tissue.

II. Experimental Methods and Materials

Steerable needles were inserted into *ex vivo* and *in vivo* liver, kidney, and prostate to study the three-dimensional shape of the needle, insertion forces, and repeatability over multiple insertions.

A. Needle Steering Robot

The needle steering robot can steer a flexible needle with an asymmetric tip by insertion and rotation of the needle shaft (Fig. 1). A similar robot is described in [9]. A rotational subsystem mounted on a translational subsystem provides the insertion and rotational motion needed for steering. The rotational subsystem consists of a 12V DC Maxon motor, an encoder and quadrature clock converter circuits, a power amplifier, and a 6-axis ATI Nano17 force-torque sensor. The translational subsystem consists of a linear slide, a 12V DC Pittman motor, an encoder, a motor control circuit to allow for manual or computer control, and a power amplifier. Computer control is performed using a Lenovo ThinkPad laptop running Ubuntu Linux 9.04 via a National Instruments PCMCIA DAQCard-6024e.

B. Animal Model

A canine model was used for both the *ex vivo* and *in vivo* experiments. The determining factor in our selection of an animal model was the need for an accurate representation of the human prostate in terms of size and pelvic anatomy. In the literature, the canine model is well established and commonly used [17]. For the *ex vivo* experiments, a set of organs (liver, kidneys, and prostate) were harvested from five fresh cadavers, obtained from an existing, unrelated non-survival experiment. Canine prostate size can vary widely based on the age, species, and size of the animal, and older, larger canines are more likely to develop enlarged prostates. As robotic needle steering could be used to treat enlarged and cancerous prostates, a larger prostate was desired for the *in vivo* experiments. One male canine (~80 kg and >5 years old) was selected for these experiments. The experiment protocol was approved by the Johns Hopkins Institutional Animal Care and Use Committee (IACUC).

C. Needle Selection and Fabrication

Three types of needles were used in the experiments: steerable nitinol bevel tip and pre-bent tip needles, and stainless steel cone tip needles (Fig. 2). The cone tip needles were used as a control to compare steerable needles to needles with straight trajectories, such as needles used in current clinical practice. Each needle type was inserted into all three organs. The needle diameters and degree of asymmetry were selected based on initial experiments in cadaveric canine livers, kidneys, and prostates to identify needles with a range of curvatures and sufficient repeatability. A needle diameter of 0.74 mm was chosen for insertions into the liver and the prostate, and a needle diameter of 0.58 mm was chosen for insertions into the kidney. A cone tip of 30° was chosen for the straight needles. A tip angle of 30° was chosen for the bevel tip steerable needles. The pre-bent tip steerable needles had a 15° pre-bent tip angle with a 30° bevel angle.

All needles were fabricated from solid wires. Cone tips were ground using a MultiPrep™ System from Allied High Tech Products, Inc., where a custom fixture held the needle at a specific angle. The needles were held at 15° to horizontal and rotated in place to create the final 30° cone tip. The bevel and bent tips were manufactured by hand, using the same procedure described in [9]. All needle tips were ground with sandpaper, increasing in grit from 180 to 300 to 600. Finally, as the surface textures of the stainless steel and Nitinol wires were different, the shafts of all needles were smoothed with 500 grit sandpaper by hand to ensure even surface texture.

D. Ex Vivo Needle Insertion Experiments

1) Experimental Setup—For *ex vivo* experiments, the robot was mounted on a pantograph mechanism as described in [9]. The organ sample was positioned on a platform and covered with a 1 mm thick latex rubber sheet secured to the platform for stabilization. The sample was also wrapped in a thin plastic cling film to prevent drying of the capsule,

leaving a small opening in the film for needle insertion. The experiments were conducted under X-ray imaging with a 9-inch XRII OEC series 9600 fluoroscope (X-ray source and CCD camera). An FTRAC, a single-image-based fluoroscope tracking fiducial, was mounted on the tissue platform to aid in pose recovery of the fluoroscope [18]. Images were acquired from the fluoroscope using a Canopus ADVC 110 frame grabber (Fig. 3).

2) Experimental Procedure—Five sets of canine organs (liver, two kidneys, and prostate from each animal) were used in these experiments. For insertions into the liver (left lateral lobe) and the prostate, each needle (cone, bevel, bent) was inserted three times in different locations, resulting in a total of 9 needle insertions per organ. For insertions into the kidney, the cone and bevel needles were inserted into one kidney, three times each, and the bent needles were inserted in the other kidney, three times each, resulting in a total of 6 insertions in one kidney and 3 in the other, for each kidney pair. This was done to minimize overlap between individual needle tracks, due the relatively small size of the kidneys. Two prostates were unusable due to small size and toughness, so a total of 27 needle insertions into prostate were recorded. Insertion speed was 0.5 cm/s for all needle insertions. Table I summarizes the *ex vivo* experiments.

3) X-Ray Stereo Reconstruction and Needle Shape Analysis—The three-dimensional shape of the needle was reconstructed from two X-ray images from a single fluoroscope, taken at −5° from vertical (left image) and +5° from vertical (right image). Background images at each fluoroscope pose were also needed for needle segmentation. As the fluoroscope available did not have position encoders, an FTRAC fluoroscope tracking fiducial and associated software was used to estimate the pose between the two stereo X-ray images. The FTRAC is accurate to approximately 0.6 mm [18]. Details of each step associated with stereo reconstruction including image calibration and rectification, pose estimation, needle segmentation, and needle pixel triangulation are described in the appendix.

For needle shape analysis, our custom Matlab program fits a circle to the needle reconstruction, eliminating outliers greater than 1.5 standard deviations away from the mean until the result converges. If convergence does not occur before all outliers are removed, program will fit a straight line to the data. The program returns the circle or line equation and a root mean squared standard error associated with the fit.

E. In Vivo Needle Insertion Experiments

1) Experimental Setup—The *in vivo* experiments took place at the Johns Hopkins Medical Institutions Radiology Research Center in an animal operating room under the guidance and supervision of a surgeon, a postdoctoral surgical fellow and multiple veterinarians and technicians.

The robot was mounted on a six-degree-of-freedom passive arm with a custom attachment (Fig. 4). Images were acquired with an Allura Xper FD20 from Philips Healthcare, a commercially available angiographic system. This system was equipped with the XperCT option, enabling C-arm cone-beam CT (CBCT) acquisition and volumetric image reconstruction [19]. For each CBCT scan, 312 projection images were acquired with the motorized C-arm. The images were reconstructed into a volumetric image dataset at 1 mm isotropic resolution for a 25 cm × 25 cm × 20 cm volume, where the 20 cm direction was the axial, z-direction.

For insertions into the prostate, the canine was placed in a supine position on the imaging table, with the hind legs pulled in towards the torso, and the robot was mounted on a movable cart in front of the perineum (Fig. 5a). After each needle insertion, the needle was

detached from the robot and the cart was moved to allow the C-arm to rotate around the canine. For insertions into the kidney, the animal was placed in a lateral position to expose the left kidney (Fig. 5b). For insertions into the liver, the animal was placed in the supine position (Fig. 5c). The robot was mounted directly on the imaging table for kidney and liver experiments. All needles and robotic components touching the animal were chemically sterilized prior to the procedure and other components were covered with sterile plastic covers.

2) Animal Preparation and Surgical Procedure—The canine was sedated, placed on a warm water circulating blanket, and then placed under full intravenous anesthesia and mechanical ventilation. Throughout the procedure, heart rate, end tidal CO2, and body temperature were monitored. The perineum, skin above the kidneys, and upper abdomen were shaved and surgically prepped before making incisions. After needle insertions for each organ, the surgical site was cleaned, all surgical towels were removed and counted, and the incision was sutured.

a) Needle Insertions in Prostate: A small incision (2 cm) was made through the tough skin of the canine's perineum to allow for needle insertions. A transrectal ultrasound probe was used along with CBCT scans and trial insertions with brachytherapy needles to locate the prostate and align the robot. A straight cone-tip needle was inserted robotically into the prostate and insertion forces were recorded. Then, the needle was detached from the robot, the robot was pulled aside, and a CBCT scan was taken. After the scan, the needle was removed manually and this process was repeated for the bevel and bent tip needles for a total of 3 needle insertions. Retraction forces were not measured.

b) Needle Insertions in Kidney: A lateral incision 5 cm below the twelfth rib was made to access the kidney. Due to the unique canine anatomy, kidney stabilization within the abdominal cavity was not possible. Rather, the kidney was carefully pulled out of the incision and stabilized with surgical towels. A straight cone-tip needle was inserted in the lower pole of kidney, along the longitudinal axis of the organ. Evans blue dye was used to mark the insertion sites to aid in histology post-mortem. During insertion, force data was collected. After insertion, a CBCT scan was taken and the needle was retracted, while recording force data. This process was repeated for the bevel and bent tip needles.

c) Needle Insertions in Liver: Access to the liver was obtained through a 10 cm midline laparotomy. A Finochietto rib spreader was used to retract the wound edges and the lobes of the liver were stabilized using surgical towels. Due to the deep chest of the canine, some lobes of the liver were not accessible; we performed one set of needle insertions in the right medial lobe and then two in the left medial lobe. A straight cone-tip needle was inserted in the left medial lobe while force data was collected. Evans blue dye was used to mark the insertion sites to aid in histology post-mortem. After insertion, a CBCT scan was taken and the needle was retracted, while recording force data. The needle was then repositioned to the right medial lobe and the process was repeated twice. The same procedure was executed for the steerable bevel and bent tip needles, resulting in a total of 9 insertions, 3 for each needle type.

Table III summarizes the types of needles used for the *in vivo* experiment. The insertion speed of all needles ranged from 0.5 cm/s to 1.5 cm/s and the retraction speed for kidney and liver was 0.5 cm/s.

After the experiments, and the animal was covered in a heated blanket to raise body temperature, as some was lost during surgery, and was taken off anesthesia and ventilation

when appropriate. The animal was monitored daily for seven days until euthanasia was required for histological analysis.

3) CBCT Needle Segmentation and Needle Shape Analysis—The scans from the Philips XperCT were converted into DICOM format and imported to Matlab for analysis. A custom Matlab program was written for semi-automated analysis of CBCT scans where the user specifies threshold levels for segmentation and defines regions containing the needle. The program then automatically fits either circles or lines to the 3D data as described in Section II-D3.

4) Tissue Health Assessment—Tissue health was assessed through blood work and histological analysis. Blood samples (10 mL) were taken several days prior to the procedure (baseline), immediately after the procedure (day 0), and on the first, third, and seventh day following the procedure. A complete blood count analysis, including white blood cells (WBC), red blood cells (RBC), hemoglobin (HGB), hematocrit (HCT), and platelets, was performed on each sample. Additional tests for liver function (bilirubin, aspartate aminotransferase (AST), alanine aminotransferase (ALT), gamma-glutamyl transferase (GGT), lactate dehydrogenase (LDH), and albumin) and kidney function (creatinine and blood urea nitrogen) were also performed. We note that when the canine arrived from the supplier, his front right paw was swollen from a previously acquired infection. Antibiotics were administered two days prior to the procedure.

The canine was euthanized on the eighth day following the procedure. The left and right medial lobes of the liver, the left kidney, and the prostate were immediately harvested and placed in a 10% formalin solution. Signs of needle entry were not evident grossly on the prostate or kidney. Faint traces of Evans blue dye were noticeable on the liver; however, no needle injury could be seen. The organs were removed from the solution after seven days and sectioned into specimens for histological analysis.

The prostate was sectioned entirely into ten specimens. Ten specimens were obtained from the upper pole of the kidney, where the needles were inserted. Ten specimens were also obtained from both the left and right medial lobes of the liver, mostly near the regions where the needles were inserted. The specimens were processed into slides using standard histologic techniques with one slide from each specimen. The slides were stained with hematoxylin and eosin to better distinguish cellular components.

III. Results

A. Experiment 1 – Ex Vivo Needle Insertion

1) Curvature Analysis—Figure 6 shows an example of original 2D X-ray images and the corresponding stereo reconstruction. The curve-fitting program fit a circle, rather than a line, to the needle shaft for 20.5% of the straight needles, for 53.9% of the bevel-tip needles, and 84.6% of pre-bent needles. With the exception of insertions of stainless steel needles into prostate, needle curvature increased with the amount of needle tip asymmetry (Fig. 7). The minimum radius curvature was 23.92 cm for straight needles, 16.45 cm for bevel needles, and 5.62 cm for pre-bent needles.

A Kruskal-Wallis non-parametric analysis of variance test was used to determine significance between groups for curvature (Table II). A p-value of less than 0.05 indicates a group has statistically significant differences; however, we note that due to unequal variance of some data groups, the Kruskal-Wallis tests has limited modeling power. To further identify which groups were significantly different from each other, a post-hoc Scheffe Test was performed using the Kruskal-Wallis test statistics. There is significantly more curvature

in pre-bent tip needles than bevel and straight needles, there is also significantly more curvature for insertions into the kidney than insertions into liver or prostate. Nitinol needles had more curvature than stainless steel needles. Finally, planes were also fit to the needle data to characterize planar deviation. The mean squared error for fitting a plane to *ex vivo* needle insertions ranged from 6.05×10^{-5} mm to 0.212 mm.

2) Force Analysis—The maximum insertion force, mean insertion force, maximum retraction force, and mean retraction force were extracted from the force data (Fig. 8). Statistical analysis was performed using the method described previously, and the results are shown in Table II. Needle type did not have a significant effect on force. Insertions into the prostate had higher maximum and mean force than insertions into kidney or liver. Maximum and mean insertion forces were higher for larger diameter needles and for stainless steel needles. The maximum and mean retraction forces for prostate were lower than for liver and the mean retraction force for liver was significantly higher than kidney as well as prostate. Stainless steel needles had lower maximum and mean retraction forces than Nitinol needles.

B. Experiment 2 – In Vivo Needle Insertion

1) Curvature Analysis—An example of a CBCT reconstruction for a needle insertion into liver with a fit curve is shown in Figure 9. In this case, a 10.4 cm circle was fit to the needle. Table III summarizes the curve fitting and the root mean squared error associated with the fit. The program fit circles, rather than lines, to 20% of the straight needles, 20% of the bevel-tip needles, and 80% of the pre-bent needles. For all insertions, the errors of fitting are on the order of the needle diameter. For cone and bevel tip needles, there was almost no curvature of the needle shaft. For bent needles, the insertion into the prostate had no curvature, however, needle insertions into the kidney and liver had radii of curvature ranging from 10.4 cm to 14.2 cm. As with *ex vivo* needle insertions, planes were fit to the data. The mean squared error of the planar fitting ranged from 0.073 mm to 0.416 mm.

2) Force Analysis—Figure 10 shows force profiles for insertions into the prostate, and insertion and retraction in the liver and kidney. The maximum and mean insertion and retraction forces were extracted from the force data and are shown in Fig. 11. Insertion forces are higher for the larger diameter needles and forces in the liver and prostate are higher than in the kidney. In addition, cone tip needles have higher insertion forces than bevel tip needles, and retractions in the liver have lower retraction forces than the kidney. For the *in vivo* experiments, there is not enough data perform statistical tests.

Some other interesting effects noticed in the data include tissue inhomogeneity, tissue relaxation [20], and delayed capsule puncture [14]. Breathing effects are also present, especially for insertions into liver. These effects increase with insertion depth. The forces due to breathing during maximum insertion of the needle had an average amplitude of 0.452 N (0.153 SD) for liver and 0.193 N (0.061 SD) for kidney. These values were found by fitting a sinusoid with the same frequency as the ventilator to the insertion force data for all needle insertions and averaging across organ groups. Breathing effects are negligible for prostate.

IV. Discussion

A. Experiment 1 – Ex Vivo Needle Insertion

The experiments in *ex vivo* tissue confirm previous experiments showing that curvature increases with increased needle tip asymmetry and that curvature increases with decreased needle diameter [9] [21]. Previous experiments in artificial tissue also indicate increased artificial tissue stiffness results in increased needle curvature as well [5], [22]. For biological

tissue, we found needle insertions into the kidney had higher curvature than prostate and liver; there is some evidence that kidney tissue is stiffer than liver tissue, which could explain this result [23]. Prostate tissue might be stiffer than kidney tissue [24]; however, additional effects due to tissue inhomogeneity and smaller organ size may explain why needles did not steer more in prostate than kidney.

The maximum and mean insertion forces for liver are comparable with previous experiments for needle insertions into *ex vivo* liver [20] [25]. Higher insertion and lower retraction force for the stainless steel needles could be due to a higher coefficient of friction for stainless steel needles. All needle shafts were ground by hand to ensure even surface texture between the needles, however, this did not necessarily equalize the coefficient of friction. Although one might expect higher insertion and retraction forces for needles with larger curvature and bent tips, no such correlation existed.

B. Experiment 2 – In Vivo Needle Insertion

The *in vivo* results for needle curvature show that pre-bent tip needles exhibit the most curvature, and bevel tip needles (without additional modification [3]) do not exhibit enough curvature to be clinically relevant. The tendency for larger diameter needles to have higher maximum and mean insertion forces could be due to larger needle surface area. High insertion forces for cone tip needles than bevel tip needles could be due to a higher coefficient of friction for stainless steel needles. This effect may not have seen in bent tip needles as interaction forces at the needle tip could have much larger than friction forces [22]. The lower retraction forces in liver as compared to kidney was a surprising result as in the *ex vivo* case, the reverse is true. The effects of blood perfusion on tissue friction for each organ could explain this result and would need further study.

Large breathing effects are evident in liver, and to a lesser extent in kidney. During many needle insertion procedures, it may not be possible to place the patient on a breath hold, so breathing forces should be considered in future needle steering development.

Qualitatively, both surgeons conducting the experiment noticed a difference between tip-asymmetric needle steering and straight needle insertions. For insertions into the prostate, it was clear that the pre-bent needle was following a curved path; however, due to tissue inhomogeneity and possible needle shape changes from detaching the needle from the robot, there was no significant curvature of the pre-bent tip needle shaft after insertion. With a thicker needle, or by using a straight introduction needle prior to insertion into the prostate, we might observe better needle curvature of a steerable needle. Additionally, haptic feedback from trial insertions with brachytherapy needles was critical to identifying prostate tissue. Thus, teleoperation for robotic needle steering could benefit from haptic cues.

1) Blood Work—Most of the blood test results remained in the normal range through day 7. The WBC was high at baseline, most likely due to the existing paw infection, and peaked on day 1. By day 7, the WBC returned to a normal level. RBC, HGB, albumin, and AST levels were abnormal following the surgery, but returned to normal levels by day 7. In general, the blood test results were consistent with expected responses to surgery, and not consistent with additional trauma that may have occurred from needle insertion.

2) Histology—Examination of the histology slides indicated no evidence of tissue damage in the majority of specimens. No evidence of acute inflammation or short term healing was apparent in prostate or liver, which would have been suggestive of an acute injury from the needle steering. In the kidney slides, inflammatory cells were present. In some slides, these cells were organized along narrow, nearly linear regions, which were likely locations of the needle tracks (Fig. 12). Neutrophils were not apparent in kidney sections, indicating a lack

of evidence for suppurative infection caused by the needle trauma. No signs of major or chronic damage were noticed.

C. Comparison of Ex Vivo and In Vivo Needle Insertion

Needles with increased tip asymmetry tend to have higher curvature in both *ex vivo* and *in vivo* tissue. In *ex vivo* tissue, insertion forces were higher in prostate than kidney and liver, which could be explained by the higher stiffness and fibrous nature of prostatic tissue. In *in vivo* tissue, insertions forces for the liver were higher than insertions into the kidney, and needle curvature was higher for pre-bent needles *in vivo* than *ex vivo*. This could be due to the fact that the vessels in the liver were perfused with blood which could have increased the overall stiffness of the tissue, as compared to the non-perfused *ex vivo* liver. Needle type did not have a significant effect on insertion or retraction forces in either ex vivo or in vivo tissue. This result is promising as it indicates that steerable needles do not exert significantly more force on tissue than straight needles. This result is confirmed further by the lack of noticeable tissue damage for steerable needles. The lack of significant planar deviation matches previously developed models of bevel-tip needle steering [7], however, more complex needle paths will most likely require some planar control for accurate targeting [26]. Finally, in both *ex vivo* and *in vivo* tissue, needle insertions into the prostate and needle insertions with bevel-tip needles did not show enough curvature to be clinically relevant.

V. Clinical Application of Needle Steering

One particularly promising application for needle steering is the treatment of large tumors with overlapping ablations. In clinical practice, complete necrosis of large tumors treated with overlapping ablations occurs in less than 50% of cases [27], primarily due to errors in placement of the ablation probe. Steerable needles can be used to improve success rates as needles can be systematically inserted, retracted, reoriented, and reinserted to reach multiple targets within an organ precisely. We used a guidewire-catheter approach: a needle was steered to a target, a Teflon tube was inserted over the needle, and a standard medical tool (e.g., a radio-frequency ablation [RFA] device) was inserted though the Teflon tube to perform a clinical relevant task (e.g., ablation). We demonstrated overlapping ablation using a tip-steerable needle and a Rita® StarBurst™ Flex RFA device in a cadaveric canine liver (Fig. 13). In these experiments, the needle insertion depths and shaft rotation angles were planned by a surgical fellow and executed by the robot, however, the accuracy of the procedure would benefit from closed loop control under CT or 3D ultrasound combined with a pre-operative ablation plan using ablation models as described in [28]. Another group has also demonstrated overlapping ablations using a different needle steering method (active cannula), using ex vivo tissue rather than *in situ* tissue, and manual insertions rather than computer-controlled insertions [11].

VI. Conclusion

We performed experiments to evaluate the differences of needle curvature and force in *ex vivo* and *in vivo* liver, kidneys, and prostate for various needle types. We compared straight needles to tip-asymmetric bevel and pre-bent needles, and found that steerable needles do not seem to damage tissue more than straight needles. In addition, insertion and retraction forces may even be lower for steerable needles than for straight needles. The minimum radius of curvature was 5.23 cm for *ex vivo* organs and 10.4 cm for *in vivo* tissue. This difference could be due to the increased stiffness and increased effect of inhomogeneity due to perfused blood vessels *in vivo*, and it indicates a need to study the effects of blood perfusion on tissue properties.

Future work includes exploring new needle designs to improve curvature and expand applicability of needle steering to other organs. Additionally, needle steering systems will need to be integrated seamlessly with existing medical imaging technology and the user interface will need to become more intuitive and natural, perhaps incorporating haptic feedback with collaborative human-robot needle control to improve needle placement.

Acknowledgments

The authors thank A. Deuget, T. Wedlick, Y. Otake, D. Scorpio, D. Ruben, L. Pipitone, R. Tunin, and J. Cook.

This work was supported by National Institutes of Health grant R01 EB006435 and a National Science Foundation fellowship. Philips Healthcare and the Johns Hopkins Medical Institutions provided access to the Allura Xper FD20. This work was performed at the Johns Hopkins University.

References

1. Abolhassani, N.; Patel, RV. Deflection of a Flexible Needle during Insertion into Soft Tissue. 28th International Conference of the IEEE Engineering in Medicine and Biology Society; 2006. p. 3858-3861.
2. DiMaio SP, Salcudean SE. Needle steering and motion planning in soft tissues. IEEE Transactions on Biomedical Engineering. 2005; 52(6):965–974. [PubMed: 15977726]
3. Engh, JA.; Podnar, G.; Khoo, SY.; Riviere, CN. Flexible Needle Steering System for Percutaneous Access to Deep Zones of the Brain. 32nd IEEE Northeast Bioengineering Conference; 2006. p. 103-104.
4. Glozman D, Shoham M. Image-Guided Robotic Flexible Needle Steering. IEEE Transactions on Robotics. 2007; 23(3):459–467.
5. Okazawa S, Ebrahimi R, Chuang J, Salcudean S, Rohling R. Hand-Held Steerable Needle Device. IEEE/ASME Transactions on Mechatronics. Jun; 2005 10(3):285–296.
6. Sears, P.; Dupont, P. A Steerable Needle Technology Using Curved Concentric Tubes. IEEE/RSJ International Conference on Intelligent Robots and Systems; 2006. p. 2850-2856.
7. Webster RJ. Nonholonomic Modeling of Needle Steering. The International Journal of Robotics Research. May; 2006 25(5–6):509–525.
8. Misra, S.; Reed, KB.; Douglas, A.; Ramesh, KT.; Okamura, AM. Needle-Tissue Interaction Forces for Bevel-Tip Steerable Needles. IEEE International Conference on Biomedical Robotics and Biomechatronics; 2008. p. 224-231.
9. Majewicz, A.; Wedlick, T.; Reed, KB.; Okamura, AM. Evaluation of needle steering in ex vivo tissue. IEEE International Conference on Robotics and Automation; 2010. p. 2068-2073.
10. Reed K, Majewicz A, Kallem V, Alterovitz R, Goldberg K, Cowan N, Okamura A. Robot-Assisted Needle Steering. Robotics & Automation Magazine, IEEE. 2011; 18(4):35–46.
11. Burdette EC, Rucker DC, Prakash P, Diederich CJ, Croom JM, Clarke C, Stolka P, Juang T, Boctor EM, Webster RJ III. The ACUSITT ultrasonic ablator: the first steerable needle with an integrated interventional tool. Work. 2010:76 290V–76 290V-10.
12. Minhas, D.; Engh, JA.; Riviere, CN. Testing of neurosurgical needle steering via duty-cycled spinning in brain tissue in vitro. International Conference of the IEEE Engineering in Medicine and Biology Society; 2009. p. 258-261.
13. Podder T, Clark D, Sherman J, Fuller D, Messing E, Rubens D, Strang J, Brasacchio R, Liao L, Ng WS, Yu Y. In vivo motion and force measurement of surgical needle intervention during prostate brachytherapy. Medical Physics. 2006; 33(8):2915. [PubMed: 16964869]
14. Yan K, Podder T, Li L, Joseph J, Rubens DR, Messing EM, Liao L, Yu Y. A real-time prostate cancer detection technique using needle insertion force and patient-specific criteria during percutaneous intervention. Medical Physics. Sep; 2009 36(9):4184–90. [PubMed: 19810492]
15. Washio, T.; Chinzei, K. Medical Image Computing and Computer-assisted Inervention (MICCAI). 2004. Needle Force Sensor, Robust and Sensitive Detection of the Instant of Needle Puncture; p. 113-120.

16. Maurin, B.; Barbe, L.; Bayle, B.; Zanne, P.; Gangloff, J.; De Mathelin, M.; Gangi, A.; Soler, L.; Forgione, A. Perspective in Image-Guided Surgery - Proceedings of the Scientific Workshop on Medical Robotics, Navigation and Visualization. Singapore: World Scientific Publishing Co. Pte. Ltd; 2004. in Vivo Study of Forces During Needle Insertions; p. 415-422.

17. Chang SC, Anthony S, Koder PC, Brown SG. Transrectal ultrasound guided manipulation of the canine prostate with minimum intervention. Lab Anim. Jul; 1997 31(3):219–224. [PubMed: 9230502]

18. Jain AK, Mustafa T, Zhou Y, Burdette C, Chirikjian GS, Fichtinger G. FTRAC - A robust fluoroscope tracking fiducial. Medical Physics. Sep.2005 32(10):3185. [PubMed: 16279072]

19. Feldkamp, La; Davis, LC.; Kress, JW. Practical cone-beam algorithm. Journal of the Optical Society of America A. Jun.1984 1(6):612.

20. Hing JT, Brooks AD, Desai JP. A biplanar fluoroscopic approach for the measurement, modeling, and simulation of needle and soft-tissue interaction. Medical image analysis. Feb; 2007 11(1):62–78. [PubMed: 17113339]

21. Webster, R., III; Memisevic, J.; Okamura, A. Design considerations for robotic needle steering. IEEE Conference on Robotics, Automation and Mechatronics, no; April; Ieee. 2005. p. 3588-3594.

22. Misra S, Reed KB, Schafer BW, Ramesh KT, Okamura aM. Mechanics of Flexible Needles Robotically Steered through Soft Tissue. The International journal of robotics research. Nov; 2010 29(13):1640–1660. [PubMed: 21170164]

23. Bensamoun SF, Robert L, Leclerc GE, Debernard L, Charleux F. Stiffness imaging of the kidney and adjacent abdominal tissues measured simultaneously using magnetic resonance elastography. Clinical imaging. 35(4):284–7. [PubMed: 21724121]

24. Zhai L, Madden J, Foo WC, Mouraviev V, Polascik TJ, Palmeri ML, Nightingale KR. Characterizing stiffness of human prostates using acoustic radiation force. Ultrasonic imaging. Oct; 2010 32(4):201–13. [Online]. Available: http://www.ncbi.nlm.nih.gov/pubmed/21213566. [PubMed: 21213566]

25. Okamura AM, Simone C, O'Leary MD. Force Modeling for Needle Insertion into Soft Tissue. IEEE Transactions on Biomedical Engineering. 2004; 51(10):1707–1716. [PubMed: 15490818]

26. Reed KB, Okamura AM, Cowan NJ. Modeling and control of needles with torsional friction. IEEE transactions on biomedical engineering. Dec; 2009 56(12):2905–16. [PubMed: 19695979]

27. Livraghi T, Goldberg SN, Lazzaroni S, Meloni F, Ierace T, Solbiati L, Gazelle GS. Hepatocellular carcinoma: radio-frequency ablation of medium and large lesions. Radiology. Mar; 2000 214(3): 761–8. [PubMed: 10715043]

28. Dodd GD, Frank MS, Aribandi M, Chopra S, Chintapalli KN. Radiofrequency thermal ablation: computer analysis of the size of the thermal injury created by overlapping ablations. AJR Am J Roentgenol. Oct; 2001 177(4):777–782. [PubMed: 11566672]

29. Sadowsky O, Lee J, Sutter EG, Wall SJ, Prince JL, Taylor RH. Enhancement of mobile C-arm cone-beam reconstruction using prior anatomical models. SPIE Medical Imaging. 2009; 7258:72 585B–72 585B12.

30. Jain A, Deguet A, Iordachita I, Chintalapani G, Blevins J, Le Y, Armour E, Burdette C, Song D, Fichtinger G. Dynamic dosimetry and edema detection in prostate brachytherapy: a complete system. Proceedings of SPIE. 2008; 6918:69, 181Y–69, 181Y–14.

31. Wedlick, T.; Okamura, A. Characterization of pre-curved needles for steering in tissue. Needle; Engineering in Medicine and Biology Society, 2009. EMBC 2009. Annual International Conference of the IEEE, no; IEEE. 2009. p. 1200-1203.

32. Mariottini G, Prattichizzo D. EGT for multiple view geometry and visual servoing - Robotics and vision with pinhole and panoramics cameras. IEEE Robotics & Automation Magazine. Dec; 2005 12(4):26–39.

Biographies

Ann Majewicz (S'04) received the B.S. degrees in Mechanical Engineering and Electrical Engineering from the University of St. Thomas, St. Paul, MN, in 2008, and the M.S. degree in Mechanical Engineering from Johns Hopkins University, Baltimore, MD, in 2010. She is currently working toward the Ph.D. degree in mechanical engineering at Stanford University, Stanford, CA.

Her research interests include needle steering, robot-assisted surgery, teleoperation, haptics, and medical simulation.

Steven P. Marra received the B.S. degree from the University of Pittsburgh in 1993, and the M.S. and Ph.D. degrees from The Johns Hopkins University, Baltimore, MD, in 1998 and 2001, respectively, all in mechanical engineering.

He is currently a Senior Lecturer in mechanical engineering at The Johns Hopkins University. His research interests include soft and hard tissue biomechanics, nonlinear mechanics of solids, mechanics of tissue damage, and undergraduate engineering education.

Mark G. van Vledder received the MSc and medical degree in 2009 at the Erasmus University Medical Center in Rotterdam, the Netherlands. He served as a research fellow in surgical oncology at the Department of Surgery in the Johns Hopkins School of Medicine, Baltimore, MD in 2009 and 2010. In 2012, he will obtain his PhD degree in surgical oncology from the Erasmus University Medical Center in Rotterdam, the Netherlands.

He is currently a resident in general surgery at the Erasmus University Medical Center, Rotterdam, the Netherlands and will continue his surgical training in the IJselland Hospital

in Capelle aan de IJssel, the Netherlands. His research interests include intraoperative ultrasound, image registration, surgical robotics, and needle based interventions for liver tumors.

Dr. van Vledder is currently a member of the Dutch Surgical Society.

MingDe Lin (M'07) received the B.S. degree from Rensselaer Polytechnic Institute, Troy, NY, in 2001, and the Ph.D. degree from Duke University, Durham, NC in 2008, all in biomedical engineering.

He is currently a Clinical Site Senior Researcher for Philips Research North America and is stationed at Johns Hopkins Hospital, Baltimore, MD since 2008 to collaborate with clinicians in developing x-ray imaging systems for interventional radiology/oncology. His research focus is in improving image quality, providing image-guided navigation tools, and quantifying therapy success in the area of hepatic carcinoma (liver cancer) treatment using transcatheter arterial chemoembolization (TACE).

Dr. Lin is the principle investigator for a National Cancer Institute grant on this work titled See, Reach, Treat, Tumor - Optimized Transarterial Chemoembolization Drug Delivery (R01 CA160771).

Michael A. Choti received the B.S. degree in Biology from the University of California, Irvine, CA, in 1979 and the M.D. from The Yale University School of Medicine. He completed a residency in General Surgery at the University of Pennsylvania, PA, in 1990, and a Fellowship in Surgical Oncology at Memorial Sloan Kettering Cancer Center, NY, in 1992. He also received the MBA in Business from Johns Hopkins University, Baltimore, MD, in 2004.

Dr. Choti is currently a Professor of Oncology, Radiology and Engineering at Johns Hopkins University, Baltimore, MD, where he is also the Jacob C. Handelsman Endowed Professor of Surgery and the Vice Chair of Clinical Affairs and Finance in the Department of Surgery. His research interests include surgical innovation, robotics, and image-guidance in cancer therapy, molecular genetics and biomarkers in colorectal and gastrointestinal cancer, and clinical trials and outcomes in gastrointestinal cancer.

Danny Y. Song received the B.S. degree in Biology from Southern Adventist University, Chattanooga, TN, in 1992 and the M.D. in 1996 from the Medical College of Georgia, Augusta, Georgia. He completed a residency in Radiation Oncology at Johns Hopkins University, Baltimore, MD in 2001.

Dr. Song serves as the Clinical Director and Director of Brachytherapy in the Department of Radiation Oncology and Molecular Radiation Sciences at Johns Hopkins University School of Medicine. He is also Co-Director of the Cancer Centers Prostate Cancer Multidisciplinary Clinic. Dr. Song's research focus is in the use of innovative guidance methods and new technologies for prostate brachytherapy to improve clinical and quality of life outcomes.

Allison M. Okamura (S'98-A'00-M'03-SM'09-F'11) received the B.S. degree from the University of California, Berkeley, in 1994, and the M.S. and Ph.D. degrees from Stanford University, Stanford, CA, in 1996 and 2000, respectively, all in mechanical engineering.

She is currently an Associate Professor of mechanical engineering at Stanford University, Stanford, CA, where she is also the Robert Bosch Faculty Scholar. She was previously Professor and Vice Chair of mechanical engineering at Johns Hopkins University, Baltimore, MD. Her research interests include haptics, teleoperation, robot-assisted surgery, tissue modeling and simulation, rehabilitation robotics, and prosthetics.

Prof. Okamura received the 2004 National Science Foundation CAREER Award, the 2005 IEEE Robotics and Automation Society Early Academic Career Award, and the 2009 IEEE Technical Committee on Haptics Early Career Award. She is an IEEE Fellow and Associate Editor of the IEEE TRANSACTIONS ON HAPTICS.

Appendix

The stereo reconstruction of needles in the *ex vivo* experiments had 5 major steps:

1. *Dewarp and Calibrate:* The needle and background images were dewarped and calibrated to correct for geometric and magnetic warping and obtain intrinsic camera parameters using the calibration phantom and methods presented in [29].
2. *Fluoroscope Pose Estimation:* The FTRAC was used to estimate the pose between the stereo image pair. First, the FTRAC positions were segmented manually using the graphical user interface from [30]. The fluoroscope pose was then found from the FTRAC positions using functions provided by the authors of [30].

3. *Needle Segmentation:* The needle was segmented from both needle images images in user-selected regions of interest. Background subtraction, top-hat filtering, and intensity adjustment highlighted the needle in the images. Connected component labeling was used to remove outliers based on the component orientation and shape, and morphological operators were used to extract needle centers in each image.

4. *Needle Pixel Correspondence:* Using a method similar to [31], pixel correspondence is found by searching along epipolar lines. In our implementation, the epipolar line was generated by using the fundamental matrix, found though the Epipolar Geometry toolbox from [32]. This process was repeated using the center needle pixels in the second image resulting in two sets of corresponding pixels – right image pixels corresponding to left image needle centers, and left image pixels corresponding to right image needle centers.

5. *Needle Pixel Triangulation:* Each set of needle points is then triangulated using methods from [30], and both sets of triangulated points are combined to define the three-dimensional needle reconstruction.

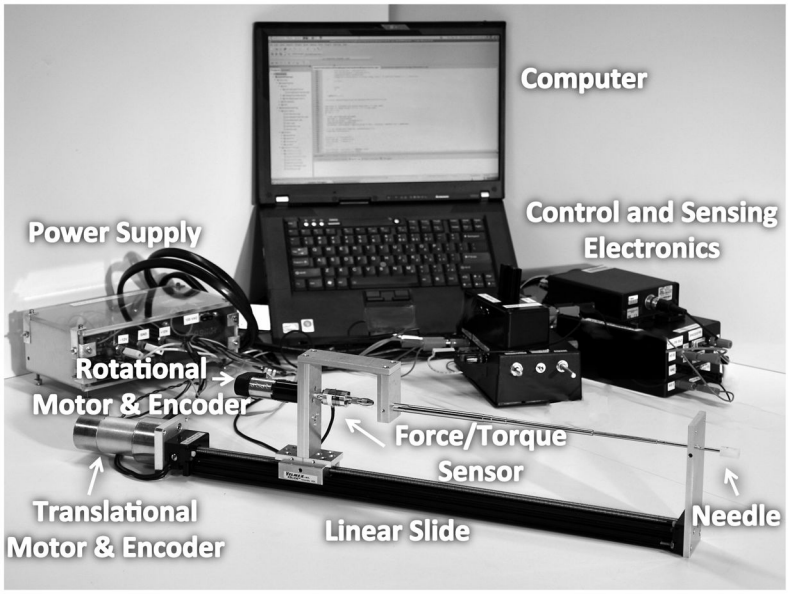

Fig. 1.
Needle steering system including the robot, computer, control and sensing electronics, and power supply.

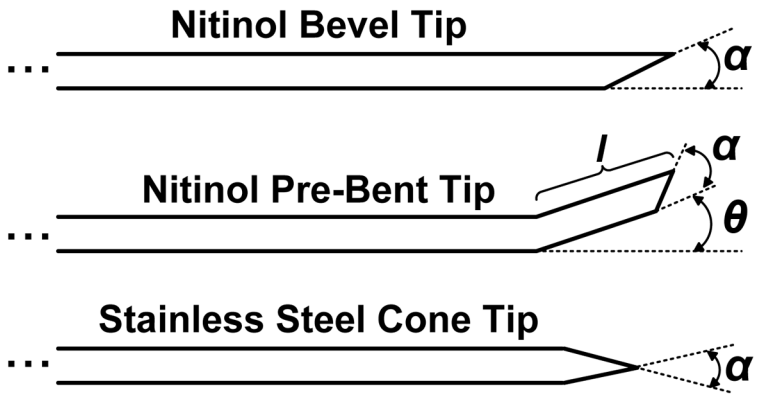

Fig. 2.

Types of needles. Bevel-tip needles have a single angled tip defined by angle α. Pre-bent needles have a bend angle θ, a bend length, l, and may also have a bevel angle. Cone-tip needles have a uniformly defined cone shaped tip defined by angle α.

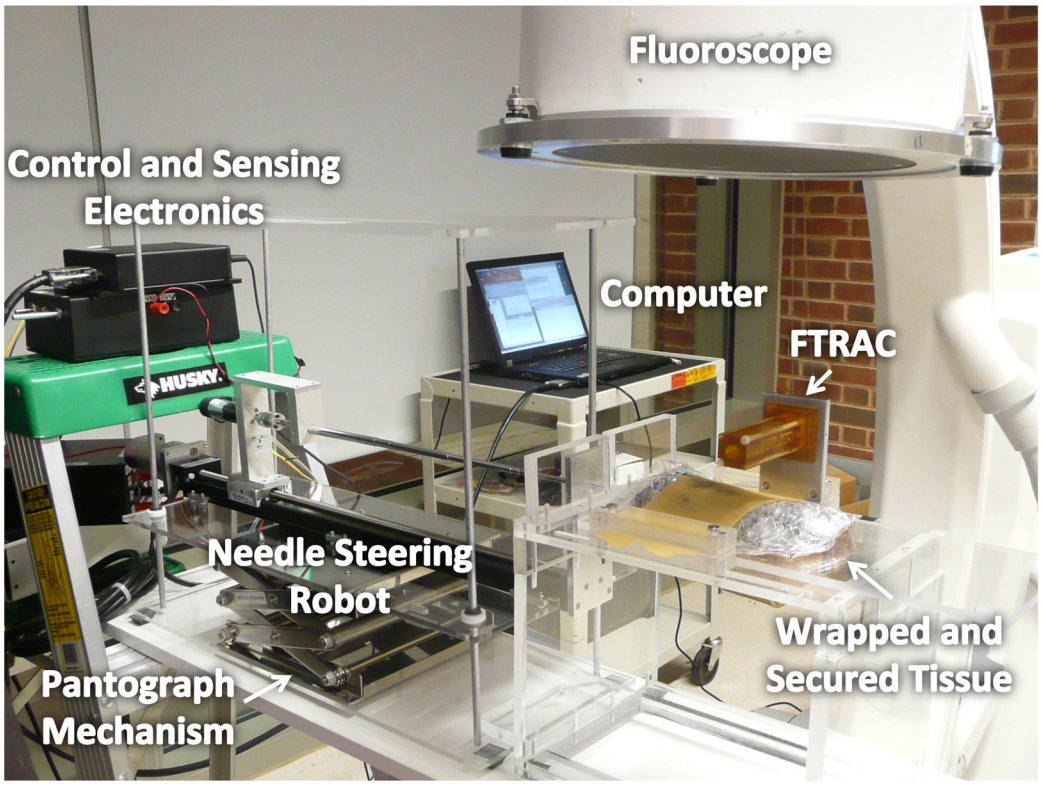

Fig. 3.
Ex vivo experimental setup. The robot was mounted on a pantograph mechanism connected to a platform supporting the tissue. The platform was positioned under a fluoroscope.

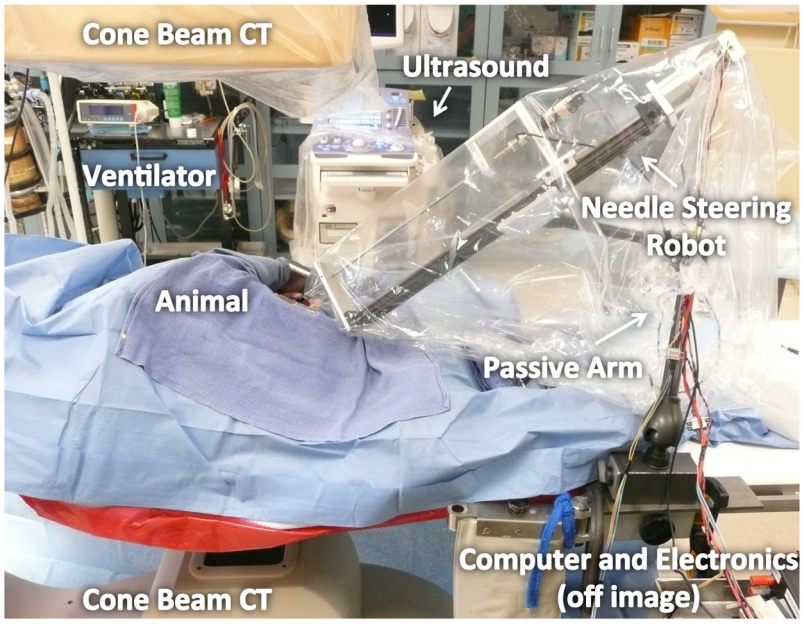

Fig. 4.

In vivo experimental setup. The robot was attached to a 6DOF passive arm, mounted either on the surgical table or a cart. The animal was placed under a C-arm CBCT scanner.

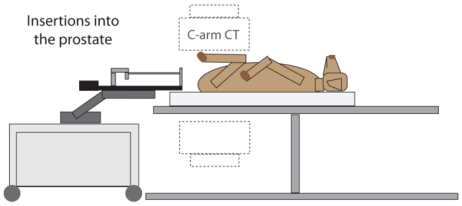

(a) Insertions into the prostate

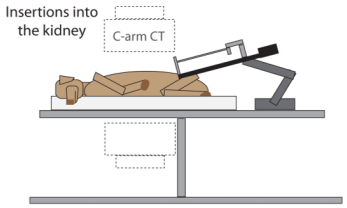

(b) Insertions into the kidney

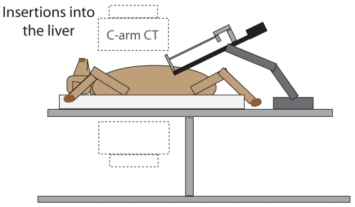

(c) Insertions into the liver

Fig. 5.

Positions of the canine during *in vivo* needle insertions into prostate (a), kidney (b), and liver (c).

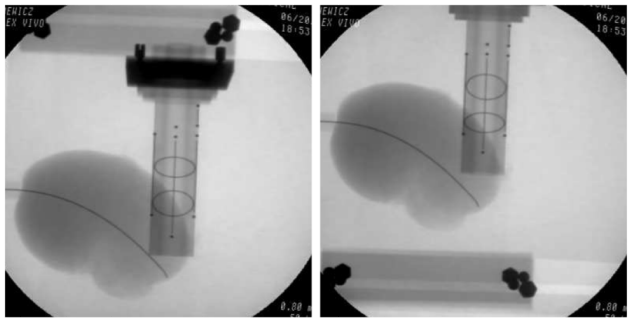

(a) Left X-Ray Image (b) Right X-Ray Image

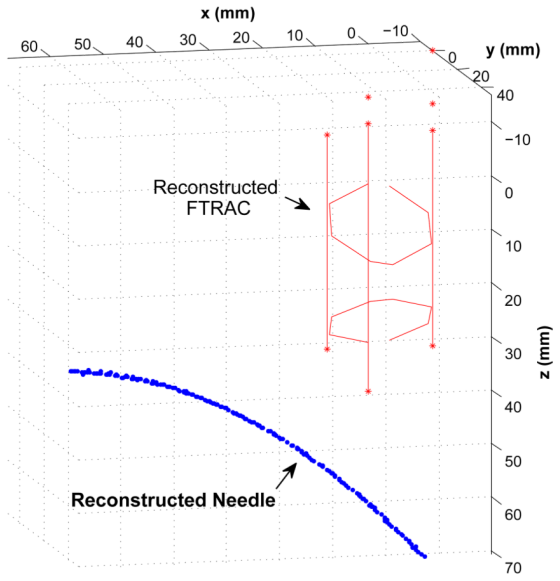

(c) 3D Needle Reconstruction

Fig. 6.

Example of stereo reconstruction (c) from stereo x-ray images (a),(b) for a needle insertion into kidney. The needle was a 0.58 mm Nitinol bent tip needle and the radius of the circle fit to the needle shaft is 7.28 cm.

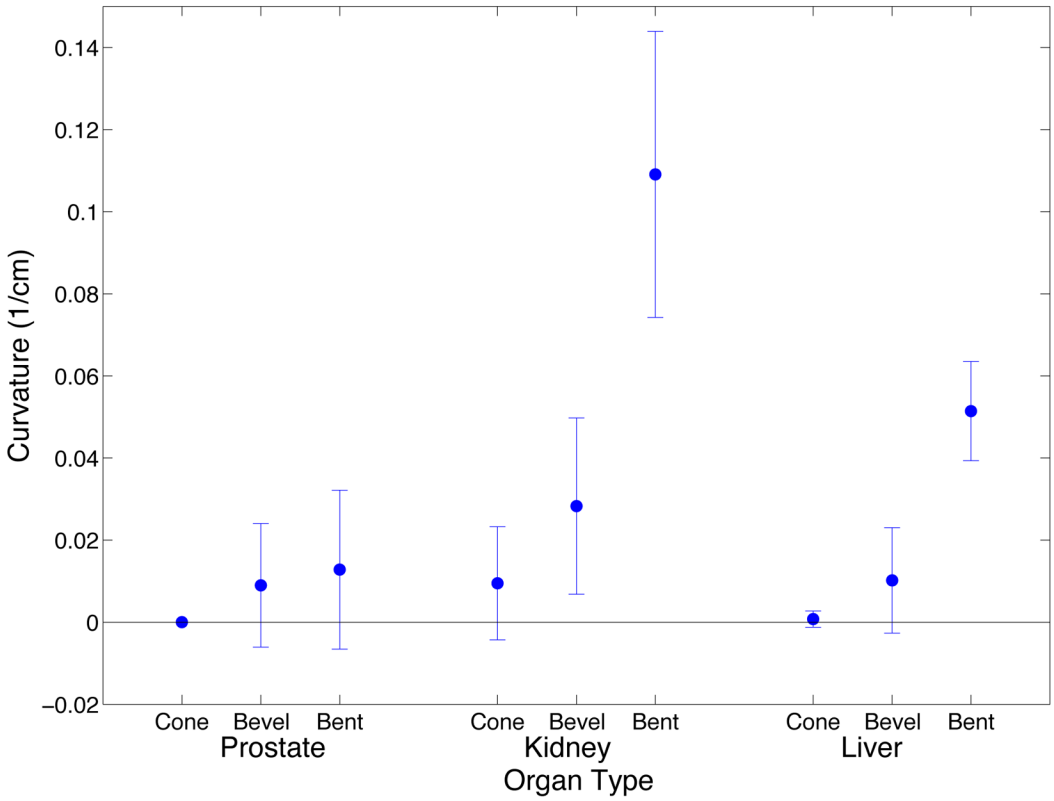

Fig. 7.

Needle curvature for cone, bevel, and bent tip needle types for insertions into prostate, kidney, and liver for *ex vivo* experiments. For liver and kidney, the mean of 15 insertions of the same needle type is shown with standard deviation error bars and for prostate the mean of 9 insertions of the same needle type is shown.

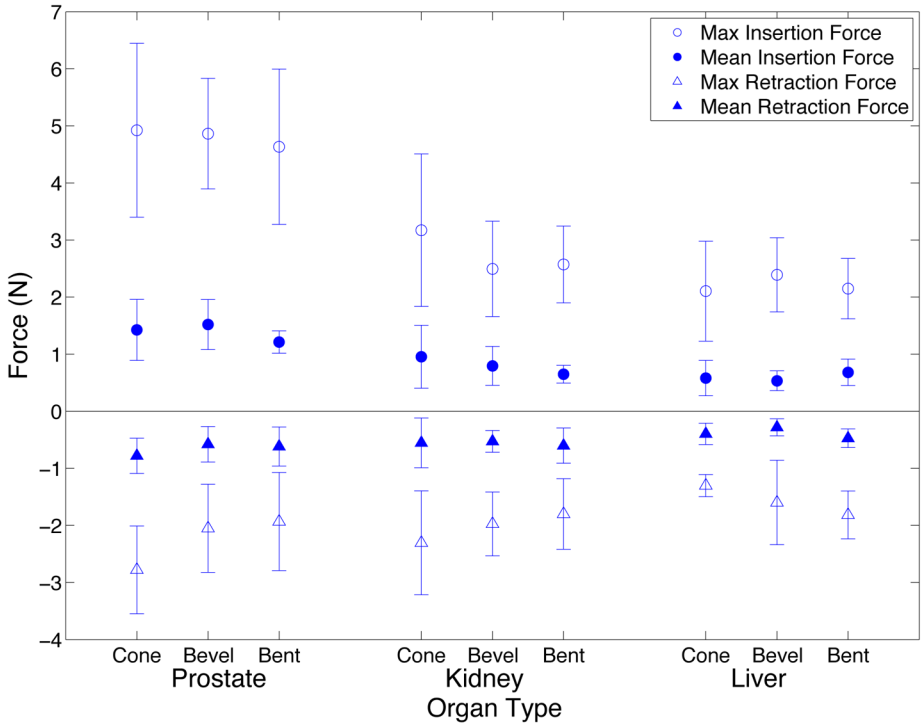

Fig. 8.

Needle insertion and retraction forces for *ex vivo* experiments. For liver and kidney, the mean of 15 insertions of the same needle type is shown with standard deviation error bars and for prostate the mean of 9 insertions of the same needle type is shown.

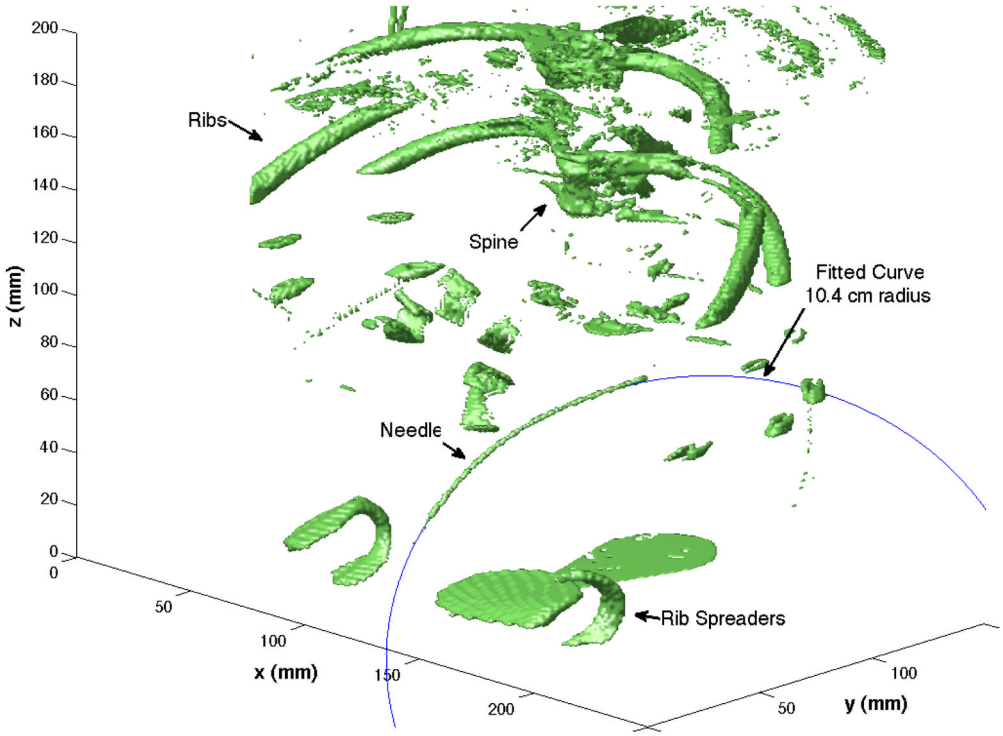

Fig. 9.
Example of curve fitting for needle insertion into liver with a 0.74 mm Nitinol bent tip needle. The radius of the fit curve is 10 .4 cm.

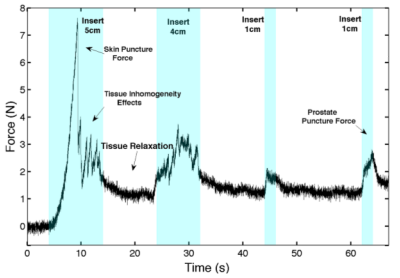

(a) Insertion Force for Cone Tip Needle in Prostate

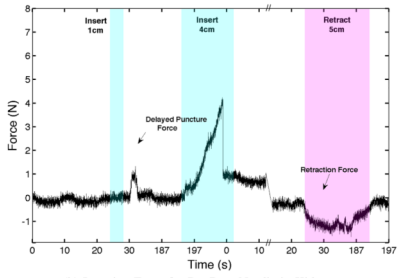

(b) Insertion Force for Pre-Bent Needle in Kidney

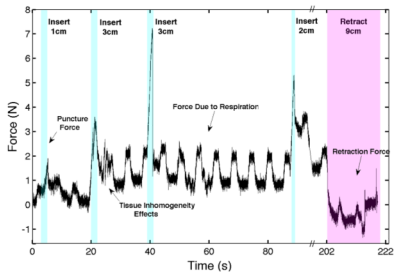

(c) Insertion Force for Pre-Bent Needle in Liver

Fig. 10.

Insertion and retraction forces during *in vivo* needle insertions into prostate, kidney, and liver. Insertion speeds ranged from 0.5 cm/s to 1.5 cm/s and the retraction speed was 0.5 cm/s.

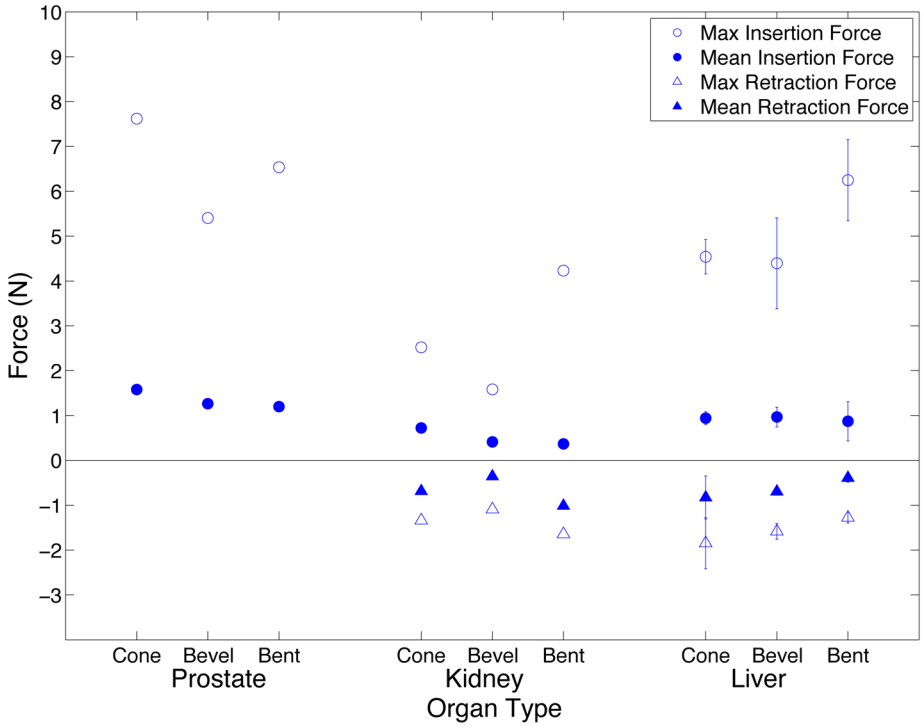

Fig. 11.

Needle insertion and retraction forces for *in vivo* experiments. For insertions into liver, the mean of three insertions of the same needle type is shown with standard deviation error bars.

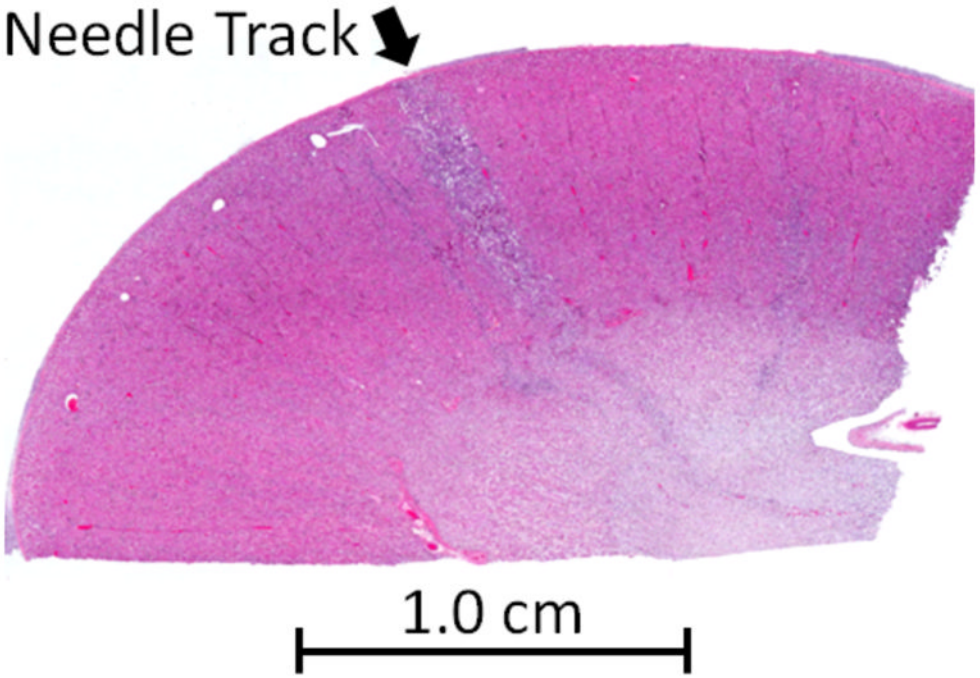

Fig. 12.
Histology section of kidney. Arrow indicates location of needle track, as evidenced by a narrow, linear region of inflammatory cells demonstrating acute healing.

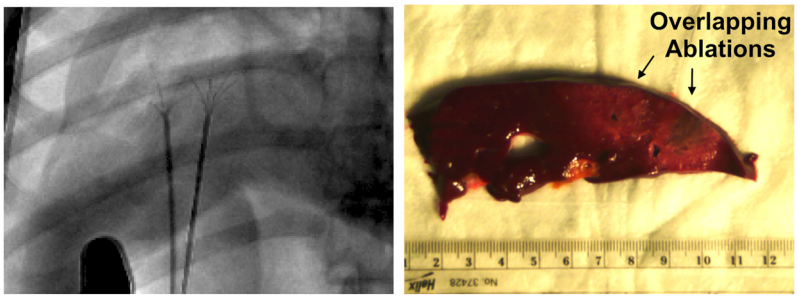

(a) Overlaid fluoroscopic images of the ablation probe

(b) Gross examination of ablation

Fig. 13.

An overlapping ablation was created using a guidewire-catheter approach for needle steering [9] to create two overlapping ablations without changing the insertion site. The needle and ablation probes were inserted under fluoroscopic guidance (a), and the ablation zones were examined in the excised liver (b).

TABLE I

Ex Vivo Needle Experiment Summary

Total # Insertions	Organ Sets Used	Organ Types	Needle Diameter (mm)
45	5	Liver	0.74
45	5	Kidney	0.58
27	3	Prostate	0.74

TABLE II

Analysis of Variance p-values for Curvature and Force in *ex Vivo* Tissue

Source	Needle Type	Organ	Needle Diameter	Needle Material
Curvature	<0.0001	<0.0001	<0.0001	0.0002
Force				
Maximum Insertion	0.5779	<0.0001	0.0190	<0.0001
Mean Insertion	0.2220	<0.0001	0.0062	<0.0001
Maximum Retraction	0.1408	<0.0001	0.5212	0.0022
Mean Retraction	0.1895	0.0002	0.2709	0.0019

TABLE III

In Vivo Curve Fitting Summary

Dataset	Needle Type	Organ	Needle Diameter (mm)	Needle Material	Insertion Distance (cm)	Fitted Curve (1/cm)*	RMSE (cm)
1	Cone	Prostate	0.74	Stainless Steel	11	$\kappa = 0.0082$	0.0521
2	Bevel	Prostate	0.74	Nitinol	12	$\kappa = 0$	0.0803
3	Bent	Prostate	0.74	Nitinol	11	$\kappa = 0$	0.0670
4	Cone	Kidney	0.58	Stainless Steel	5	$\kappa = 0$	0.0943
5	Bevel	Kidney	0.58	Nitinol	5	$\kappa = 0$	0.0782
6	Bent	Kidney	0.58	Nitinol	5	$\kappa = 0.0952$	0.0532
7, 8, 9	Cone	Liver	0.74	Stainless Steel	7, 9, 8	$\kappa = 0$, $\kappa = 0$, $\kappa = 0$	0.1073, 0.0649, 0.0890
10, 11, 12	Bevel	Liver	0.74	Nitinol	9, 9, 9	$\kappa = 0$, $\kappa = 0$, $\kappa = 0$	0.0603, 0.1099, 0.0840
13, 14, 15	Bent	Liver	0.74	Nitinol	7, 10, 9	$\kappa = 0.0730$, $\kappa = 0.0704$, $\kappa = 0.0962$	0.0480, 0.0441, 0.0527

*$\kappa = 0$ indicates that a line was a better fit to the data than a circle.

IEEE Trans Biomed Eng. Author manuscript; available in PMC 2013 September 01.